IJMMM International Journal of Minerals, Metallurgy and Materials 矿物冶金与材料学报（英文版）

Oxidation behavior of high Hf nickel-based superalloy in air at 900, 1000 and 1100°C

Jiu-han Xiao, Ying Xiong, Li Wang, Xiang-wei Jiang, Dong Wang, Kai-wen Li, Jia-sheng Dong, and Lang-hong Lou

Cite this article as:
Jiu-han Xiao, Ying Xiong, Li Wang, Xiang-wei Jiang, Dong Wang, Kai-wen Li, Jia-sheng Dong, and Lang-hong Lou, Oxidation behavior of high Hf nickel-based superalloy in air at 900, 1000 and 1100°C, *Int. J. Miner. Metall. Mater.*, 28(2021), No. 12, pp. 1957-1965. https://doi.org/10.1007/s12613-020-2204-z

View the article online at SpringerLink or IJMMM Webpage.

Articles you may be interested in

Ya Wei, Yu Fu, Zhi-min Pan, Yi-chong Ma, Hong-xu Cheng, Qian-cheng Zhao, Hong Luo, and Xiao-gang Li, Influencing factors and mechanism of high-temperature oxidation of high-entropy alloys: A review, *Int. J. Miner. Metall. Mater.*, 28(2021), No. 6, pp. 915-930. https://doi.org/10.1007/s12613-021-2257-7

Jun-jun Yan, Xue-fei Huang, and Wei-gang Huang, High-temperature oxidation behavior of 9Cr5Si3Al ferritic heat-resistant steel, *Int. J. Miner. Metall. Mater.*, 27(2020), No. 9, pp. 1244-1250. https://doi.org/10.1007/s12613-019-1961-z

Zhi-yuan Zhu, Yuan-fei Cai, You-jun Gong, Guo-ping Shen, Yu-guo Tu, and Guo-fu Zhang, Isothermal oxidation behavior and mechanism of a nickel-based superalloy at 1000, *Int. J. Miner. Metall. Mater.*, 24(2017), No. 7, pp. 776-783. https://doi.org/10.1007/s12613-017-1461-y

Adam Khan Mahaboob Basha, Sundarrajan Srinivasan, and Natarajan Srinivasan, Studies on thermally grown oxide as an interface between plasma-sprayed coatings and a nickel-based superalloy substrate, *Int. J. Miner. Metall. Mater.*, 24(2017), No. 6, pp. 681-690. https://doi.org/10.1007/s12613-017-1451-0

Pan-jun Wang, Ling-wei Ma, Xue-qun Cheng, and Xiao-gang Li, Influence of grain refinement on the corrosion behavior of metallic materials: A review, *Int. J. Miner. Metall. Mater.*, 28(2021), No. 7, pp. 1112-1126. https://doi.org/10.1007/s12613-021-2308-0

Saeed Aliakbari Sani, Hossein Arabi, Shahram Kheirandish, and Golamreza Ebrahimi, Investigation on the homogenization treatment and element segregation on the microstructure of a /'-cobalt-based superalloy, *Int. J. Miner. Metall. Mater.*, 26(2019), No. 2, pp. 222-233. https://doi.org/10.1007/s12613-019-1727-7

IJMMM WeChat

QQ author group

International Journal of Minerals, Metallurgy and Materials
Volume 28, Number 12, December 2021, Page 1957
https://doi.org/10.1007/s12613-020-2204-z

Oxidation behavior of high Hf nickel-based superalloy in air at 900, 1000 and 1100°C

Jiu-han Xiao[1,2], *Ying Xiong*[3], *Li Wang*[1], *Xiang-wei Jiang*[1], *Dong Wang*[1], *Kai-wen Li*[1], *Jia-sheng Dong*[1], *and Lang-hong Lou*[1]

1) Shi-Changxu Innovation Center for Advanced Materials, Institute of Metal Research, Chinese Academy of Sciences, Shenyang 110016, China
2) School of Materials Science and Engineering, University of Science and Technology of China, Shenyang 110016, China
3) China National South Aviation Industry Company Limited, Zhuzhou 412002, China
(Received: 15 July 2020; revised: 28 September 2020; accepted: 30 September 2020)

Abstract: To investigate the oxidation behavior of a nickel-based superalloy with high hafnium content (1.34wt%), this study performed isothermal oxidation tests at 900, 1000, and 1100°C for up to 200 h. X-ray diffraction and scanning electron microscopy with energy-dispersive X-ray spectroscopy were applied to study the oxidation behavior. The weight gain of the high Hf nickel-based superalloy exhibited a parabola-like curve, and no spallation of the oxide scale was observed during the oxidation tests. The alloy presented excellent oxidation resistance, and no HfO_2 was observed in the oxide scale at 900°C. With the increase of the oxidation temperature to 1000°C, HfO_2 particles formed in the spinel phases of the scale, and "peg-like" HfO_2 was observed within and beneath the inner layer of Al_2O_3 after 200 h. As the oxidation temperature rose to 1100°C, "peg-like" HfO_2 was observed at the early stage of the oxidation test (within 25 h). The formation mechanism of HfO_2 and its impact on oxidation resistance were investigated based on the analysis of the oxidation test results at different temperatures.

Keywords: superalloy; hafnium; high-temperature oxidation; diffusion

1. Introduction

Nickel-based superalloys have been widely applied to manufacture the blades and vanes of aero engines and gas turbines because of their outstanding oxidation resistance, superior corrosion resistance, and excellent mechanical capacities at high temperatures. For improving service temperatures, large amounts of refractory elements (such as W, Mo, Re, Hf, and Ta) have been mixed into newly developed superalloys. The large atomic radii of these refractory elements can enhance the solution strengthening effect for alloys. Moreover, the addition of refractory elements increases the melting points of alloys and reduces the cation diffusion ability. These effects can also improve mechanical properties at elevated temperatures. The influences of W, Mo, Ta, and Re on the performances of superalloys have been extensively investigated [1–4], but the effects of Hf have been rarely reported in the open literature [5–8].

In general, Hf is a grain boundary strengthening element that forms dispersed HfC along grain boundaries. HfC can prevent the movement of dislocation and, thus, pin the grain boundaries to keep them from sliding, which greatly improves the creep resistance of superalloys at high temperatures. The hardness and liquidity of superalloys can also be increased remarkably by HfC. Therefore, high Hf content helps improve the service and casting properties of superalloys [9–10]. However, Hf also exerts detrimental effects on Ni-based superalloys. For example, the interface reaction between molten alloy and ceramic shell at high temperatures can be promoted with the addition of Hf, thereby increasing the risk of the formation of surface defects and impurities [11–13]. At present, most researches on the effects of Hf is mainly focused on the oxidation resistance and adherence of coatings and, thus, few research explored the high Hf content of alloys [14–19]. Hf is widely known to benefit oxidation resistance. Remarkable improvements in the adherence of oxide scales have been made through the addition of Hf to coatings [14−16]. However, limited studies have investigated the effects of high Hf content on the oxidation resistance of Ni-based superalloys. Related studies have reported that the quantity of Hf in commercial nickel-based superalloys is relatively low (usually 0 or <0.4wt%) [20−21]. Additionally,

Corresponding author: Dong Wang E-mail: dwang@imr.ac.cn
© University of Science and Technology Beijing 2021

the effects of high Hf content on oxidation resistance are not systematically investigated. To evaluate the oxidation behavior of high hafnium superalloys, the current work conducted oxidation tests on a Ni-based superalloy with 1.34wt% Hf at 900, 1000, and 1100°C. The oxidation behavior of a Ni-based superalloy with high Hf content was evaluated and discussed accordingly.

2. Experimental

The alloy was prepared in a vacuum induction melting furnace and casted into cylindrical rods by pouring the liquid alloy into a ceramic shell mold prepared by the lost wax technique. The chemical composition of the high Hf nickel-based superalloy is listed in Table 1. In order to eliminate casting defects, reasonable melting parameters should be adopted. The shell mold was prebaked at 1100°C for 4 h. Meanwhile, the ingot was heated up to 1420°C and held for 10 min until complete melting was observed. The alloy was solution heat treated at 1185°C for 2 h, air cooled, and then aged including two steps: at 1050°C for 4 h, followed by air cooling, and then at 870°C for 20 h, followed by air cooling. The oxidation specimens measuring 10 mm × 20 mm × 1.5 mm were cut with an electro-discharge machine. All the specimens were grounded with 1000-grit sandpaper under water and then ultrasonically cleaned in acetone for 5 min before the oxidation tests. At the same time, corundum crucibles were presintered at 1200°C for 100 h.

Table 1. Chemical composition of the high Hf nickel-based superalloy wt%

Ni	Co	Cr	Al + Ti	W + Mo	Ta	Hf	C	B	Zr
Bal.	10.02	8.37	6.42	10.60	3.03	1.34	0.13	0.02	0.01

Oxidation tests were performed at 900, 1000, and 1100°C in accordance with the service temperature of the high Hf nickel-based superalloy for up to 200 h in air. The weight gain of the specimens was measured after 25, 50, 75, 100, 125, 150, 175, and 200 h, and the typical specimens (oxidation interrupted after 1, 5, 25, 100, and 200 h) were selected for analysis. The test specimens were weighted with an analytical balance with a sensitivity of 10^{-4} g to ensure the accuracy of the experiment. The average value of the weight gained from three equivalent specimens in this study was calculated to reduce error propagation under the same conditions. The weighed data were unified into the unit of mg/cm^2 to confirm the specific weight change.

The oxidation products were analyzed by X-ray diffraction (XRD). The surface and cross sections of the oxidized specimens were observed and analyzed by scanning electron microscopy (SEM) equipped with energy-dispersive X-ray spectroscopy and backscatter detectors.

3. Results

3.1. Oxida tion kinetics curves

The curves of weight gain as a function of thermal exposure time for the high Hf nickel-based superalloy at 900, 1000, and 1100°C are plotted in Fig. 1. Weight gain throughout the whole oxidation process at different temperatures was observed, and the weight increment increased with the oxidation temperature. The oxidation kinetics curve at each oxidation temperature roughly followed the parabolic law. As the oxidation temperature rose, the rate of initial oxidation increased, and the weight gain of oxidation became increasingly obvious.

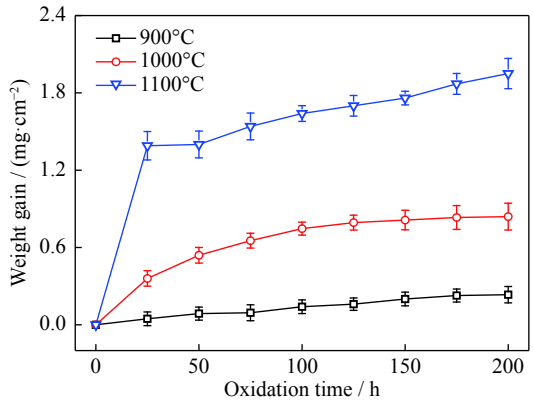

Fig. 1. Oxidation kinetics curves of the high Hf nickel-based superalloy after oxidation at 900, 1000, and 1100°C.

The average weight gain of the high Hf nickel-based superalloy was about 1.95 mg/cm^2 for 200 h at 1100°C. This value was about twice that obtained with isothermal oxidation at 1000°C (0.84 mg/cm^2) and nine times that obtained with isothermal oxidation at 900°C (0.23 mg/cm^2). The comparison of these results with the aforementioned sets of data reveals the obvious rule.

3.2. Identification of oxidation products

XRD analysis was performed to identify the oxidation products. Fig. 2 shows the XRD results of the original and oxidized specimens at 900, 1000, and 1100°C for 200 h. The diffraction spectrum shows that oxidation products scarcely formed at 900°C. At 1000°C, the oxidation products were mainly composed of Al_2O_3, HfO_2, CrO, and two types of spinel phases ($(Ni,Cr,Ti)(Cr,Co)_2O_4$ and $(Ta_2O_5)_{15}(WO_3)_2$). At 1100°C, the amount of oxidation products increased, and HfO_2 was observed.

3.3. Surface morphology and chemical composition

Fig. 3 shows the surface morphology of the high Hf nickel-based superalloy thermally exposed at 900, 1000, and 1100°C for 200 h. The specimen surfaces still presented some metallic gloss, and a few white lumpy particles were

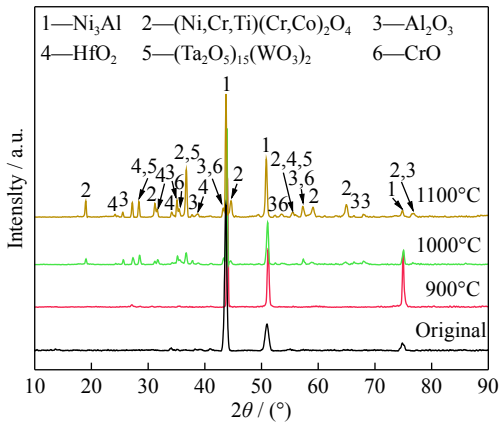

Fig. 2. XRD spectra of the high Hf nickel-based superalloys under different oxidation conditions (original and oxidized at 900, 1000, and 1100°C for 200 h).

dispersed on the surface (Figs. 3(a)–3(c)). This result indicated that only a slight oxidation reaction occurred on the surface of the high Hf nickel-based superalloy at 900°C. At 1000°C, two types of surface morphology (light gray and dark gray) were observed (Figs. 3(d)–3(f)). This feature implied the occurrence of a more serious oxidation than that observed in the specimens oxidized at 900°C. Figs. 3(g)–3(i) show a highly complex and serious surface oxidation at 1100°C.

3.4. Scale morphology and element distribution

The cross sections of the oxidized specimens were observed. Fig. 4 shows the backscattered electron images and distribution maps of the major elements on the cross section of the high Hf nickel-based superalloy oxidized at 900°C for 200 h. An oxide layer formed on the surface of the specimen, and no γ′ depletion zone was found (Fig. 4(a)). Two typical regions, namely, noncarbide region and carbide region, were selected for measurement. A discontinuous scale rich in Al, Cr, and O was observed (Fig. 4(b)). These results, in combination with those of the XRD, indicate the formation of a discontinuous oxide layer composed of Al_2O_3 and CrO on the surface of the specimen in the noncarbide region. The thickness of the oxide scale was about 2.5 μm. However, in the carbide region, the oxidation process was accelerated by interdendritic MC carbides (Fig. 4(c)). Unlike noncarbide regions, the carbide region did not show an Al-rich surface. Al cations diffused along the interface of the carbides and matrix and reacted with the O anions to form Al_2O_3 surrounding the carbides. Meanwhile, the oxides of W, Ta, Hf, and Ti could be traced to the oxidized MC carbides. The depth of the inward diffusion of the O anions reached 14 μm. Owing to the excellent oxidation resistance of the alloy at 900°C, a slow weight gain was observed, and this condition led to a low-slope and flat oxidation kinetics curve (Fig. 1).

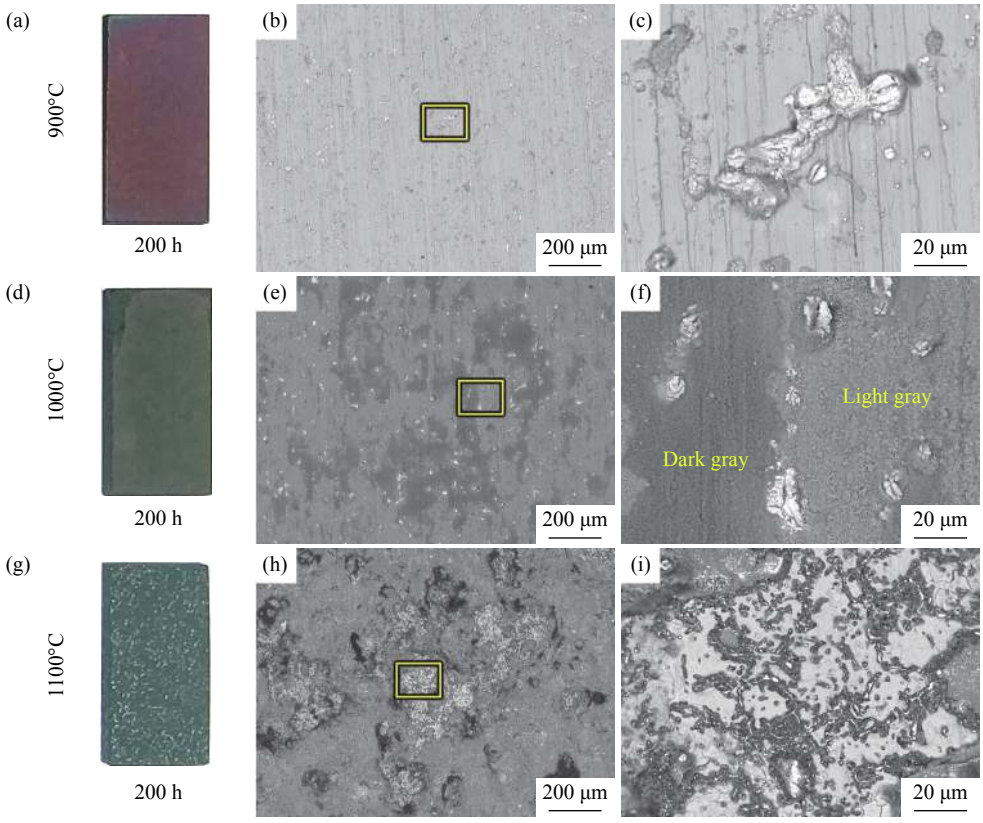

Fig. 3. Macroscopic images (a, d, g) and SEM surface micrographs (b, c, e, f, h, i) of the high Hf nickel-based superalloy after 200 h of oxidation at 900°C (a–c), 1000°C (d–f), and 1100°C (g–i).

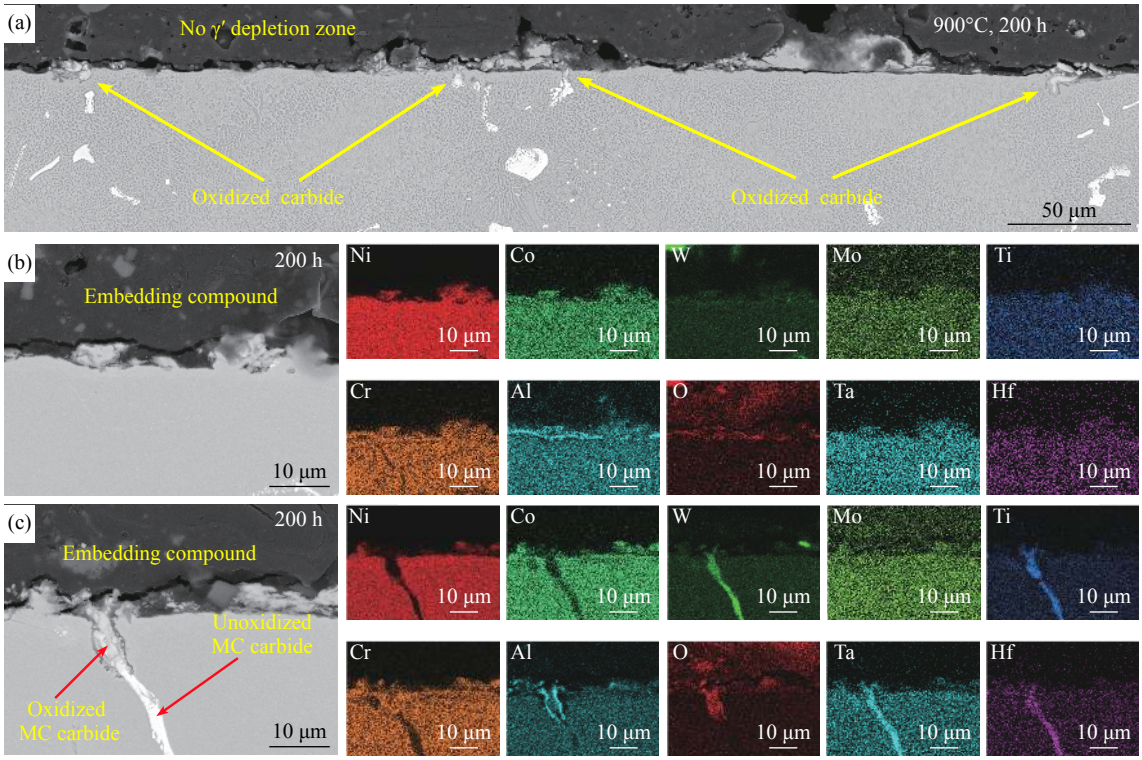

Fig. 4. SEM backscattered electron micrographs and element distribution maps of cross section of the high Hf nickel-based superalloy after oxidation at 900°C for 200 h: (a) microstructure morphology at low magnification; (b) noncarbide region; (c) carbide region.

The cross sections of the oxide scales of the high Hf nickel-based superalloy oxidized at 1000°C are shown in Fig. 5. Only a thin oxide scale was observed after oxidation for 5 h. A light gray oxidation product wrapped in a grayish-white phase appeared in the oxide scale after 100 h of oxidation. Moreover, a dark gray layer continuously precipitated in the inner oxide scale. After oxidation for 200 h, the oxide scale deepened, and a fine strip-like bright phase surrounded by a dark gray phase precipitated in the matrix below the oxidation layer. A thin oxide layer (Al_2O_3) is usually observed around carbides because of the selective oxidation of Al [22–23]. Herein, a large number of bright white oxidation products were found in the vicinity of the oxidized MC carbide after oxidation for 200 h.

Fig. 6 shows the microstructure micrographs and element distribution of the cross section of the high hafnium superalloy oxidized at 1000°C for 200 h. The surface of the specimen was covered by a continuous oxide layer, and an obvious γ′ depletion zone appeared under the oxide scale (Fig. 6(a)). The thickness of the γ′ depletion zone was about 15 μm. Some of the interdendritic MC carbides exposed on the surface were oxidized; they are marked as yellow arrows in Fig. 6(a). As shown in Fig. 6(b), the oxide scale was divided into the outer and inner layers. The outer oxide layer was complex and mainly composed of a Ni, Co, Cr, and Ti-rich phase, W and Ta-rich phase, and Hf-rich oxide. Based on these results, along with the XRD results, the oxidation products were determined as $(Ni,Cr,Ti)(Cr,Co)_2O_4$, $(Ta_2O_5)_{15}(WO_3)_2$, and HfO_2. The dark gray phase located in the inner oxide layer was identified as Al_2O_3. The bright white phase embedded in Al_2O_3 was confirmed as HfO_2. In the carbide region, the blocky MC carbides underwent an oxidation reaction and formed HfO_2 *in situ*. Moreover, an Al_2O_3 layer was found on the outer surface (Fig. 6(c)). The diffusion of Hf cations was more active during oxidation at 1000°C than during oxidation at 900°C. Additionally, HfO_2 was formed within the outer oxide layer and beneath the inner layer. The oxidation of the alloy was aggravated, and the protective oxide layer was established gradually at this moment, resulting in a smooth parabola of the oxidation kinetics curve (Fig. 1).

The microstructure of the high hafnium superalloy after oxidation at 1100°C is shown in Fig. 7. The oxide scale of about 5 μm was formed after 1 h of oxidization. The thickness of the oxide scale increased after oxidation for 5 h. A few bright white particles (HfO_2) precipitated beneath the inner oxide layer after oxidation for 25 h. The amount of HfO_2 that precipitated under the oxide scale increased with the increase of the oxidation time to 200 h. The precipitated HfO_2 phase tended to extend inward in the direction perpendicular to the specimen surface. Serious oxidation occurred along the grain boundary, and the depth of the oxidized grain bound-

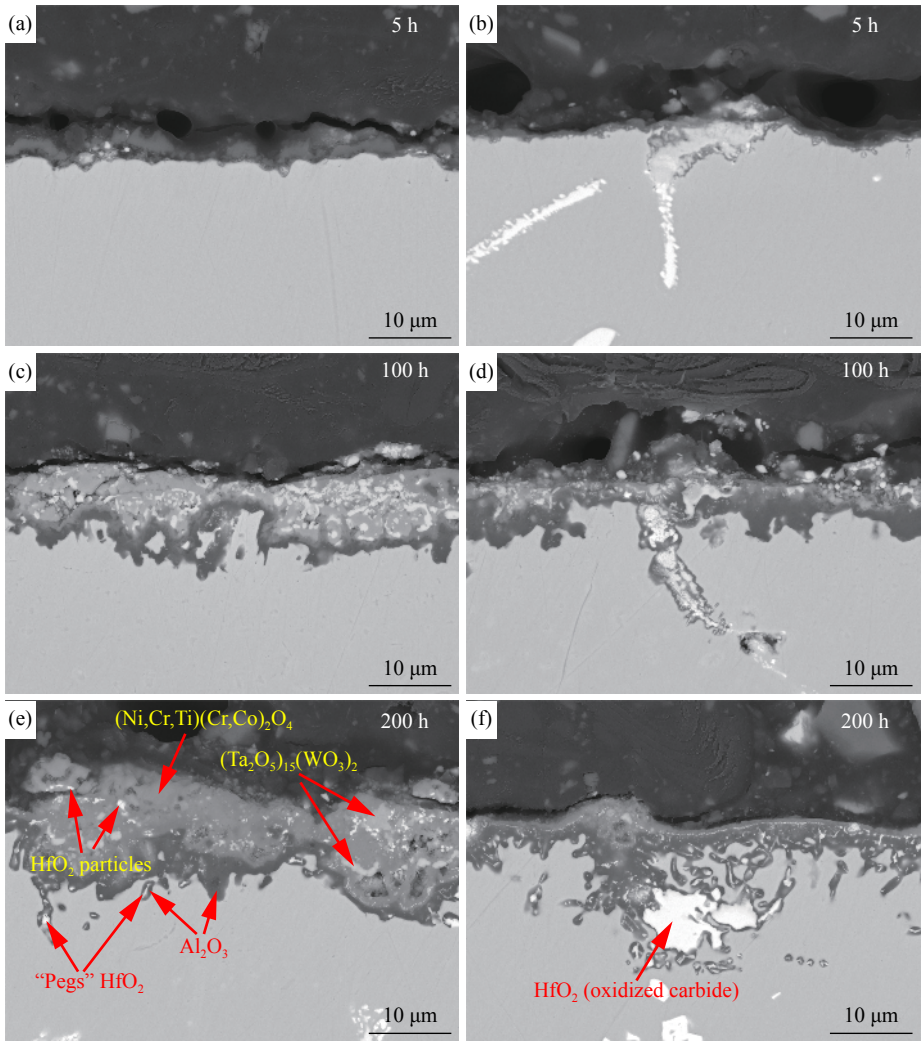

Fig. 5. SEM backscattered electron micrographs of cross section of the high Hf nickel-based superalloy after oxidation at 1000°C for 5, 100, and 200 h: (a, c, e) noncarbide region; (b, d, f) carbide region.

ary reached 50 μm (Fig. 7(f)).

Fig. 8 shows the element distribution maps of the cross section of the high Hf nickel-based superalloy after oxidation at 1100°C for 200 h. A limited number of oxidized interdendritic carbides were observed on the surface, and a relatively thick γ′ depletion zone (approximately 40 μm) was found beneath the oxide layer (Fig. 8(a)). Therefore, the oxidation at 1100°C was dominated by uniform diffusion, and a large number of Al atoms in the γ′ phase diffused to the surface oxide scale. Compared with the oxidation at 1000°C, the oxidation at 1100°C presented a great increase in oxide thickness and resulted in the embedding of many strip-like HfO_2 surrounded by Al_2O_3 in the matrix. This result implied that Hf cations were more active and diffused much faster at 1100°C than at 1000°C. Before the first 25 h of oxidation at 1100°C, the stable protective layer was not established completely, thereby leading to the significant weight gain of the alloy. Subsequently, the weight gain increased slowly when the stable oxide scale on the matrix formed. The corresponding oxidation kinetics curve is shown in Fig. 1.

4. Discussion

The experimental results clearly showed that the addition of Hf element exerted different effects on the oxidation behavior of the high Hf nickel-based superalloy at different temperature. For isothermal oxidation at 900°C, the Hf cations showed no obvious diffusion, but the MC carbides showed oxidation. On the one hand, this result is attributed to the low thermodynamic driving force and high barrier energy for the diffusion of Hf cations at a relatively low temperature. According to the recent literature and thermodynamic software calculations (Outotec HSC Chemistry), the equilibrium Gibbs free energy of the reactions shown in Eqs. (1)–(3) are negative at 900°C [24–26].

$$\frac{4}{3}Al + O_2 = \frac{2}{3}Al_2O_3 \quad (1)$$

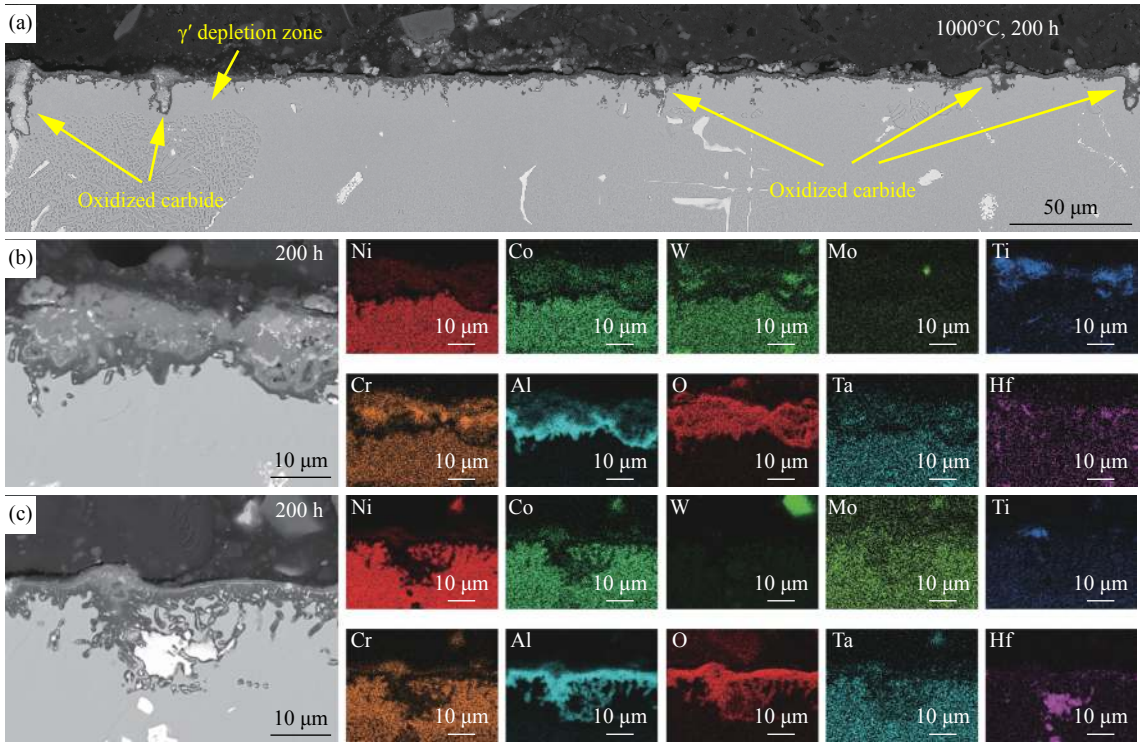

Fig. 6. Element distribution maps of cross section of the high Hf nickel-based superalloy after oxidation at 1000°C for 200 h: (a) microstructure morphology at low magnification; (b) noncarbide region; (c) carbide region.

$$4Cr + 5O_2 = 2Cr_2O_5 \quad (2)$$

$$Hf + O_2 = HfO_2 \quad (3)$$

Hence, the reactions to form Al_2O_3, CrO, and HfO_2 can theoretically occur. However, because the cationic radius of Hf is larger than those of Cr and Al, the diffusion barrier energy of Hf cations is higher than those of Al and Cr cations. This characteristic leads to a faster outward diffusion of Al and Cr cations than Hf cations from an oxide layer. The oxide scale of Al and Cr on the surface can prohibit the further diffusion of oxygen anions into the metal matrix to generate HfO_2 [27–28]. However, the atomic arrangement of MC carbides that precipitated in the interdendrite during the solidification process was different from that of the surrounding matrix. This lattice mismatch caused the energy to rise at the carbide/matrix interface [29]. Hence, oxygen could diffuse rapidly inward to oxidize MC carbides through the high energy interface of the carbide/matrix. At this point, quantities of active Al cations in the γ′ phase also diffused to the carbide/matrix interface and combined with oxygen to form Al_2O_3. As a result, the Al_2O_3 layer on the surface disappeared in the carbide region.

The mutual diffusion between the reactive element cations and the oxygen anions became more serious at 1000°C than at 900°C. The diffusion coefficient of Hf increases at a high oxidation temperature according to the following Arrhenius formula [30]:

$$D = D_0 \exp\left(-\frac{Q}{RT}\right) \quad (4)$$

where D is the diffusion coefficient, D_0 is the pre-exponential factor, Q is the diffusion activation energy, R is the gas constant, and T is the diffusion temperature. In this formula, D_0 and Q are constants related to alloy composition. R is a constant equal to 8.314 J/(mol·K). Thus, diffusion coefficient D increases as temperature T increases. In addition to the significant outward diffusion and local segregation of Hf cations within and beneath the oxide scale, blocky MC carbides were completely oxidized for HfO_2 formation. HfO_2 was dispersedly distributed in the outer spinel phase within 100 h. Previous studies have suggested that reactive elements (such as Hf) are prone to segregation at grain boundaries and to reaction with oxygen anions that diffuse inward along the grain boundaries to form HfO_2 [31–36]. The latter view was contested by Cao *et al.*, who reported the oxidation mechanism of HfO_2 particles in the spinel, specifically in this mechanism, Hf cations dissolved in the matrix are oxidized *in situ* by oxygen anions that diffuse inward, and the continuous outward diffusion of Hf cations in the matrix driven by the oxygen potential gradient make HfO_2 particles coarse [37–39]. With respect to the bright white HfO_2 phase that resembled "pegs" beneath the inner layer of Al_2O_3 in this work, the formation mechanism is different from that in spinel. As a result of the existence of an external diffusion driving force, the Hf cations dissolved in the matrix easily diffused out-

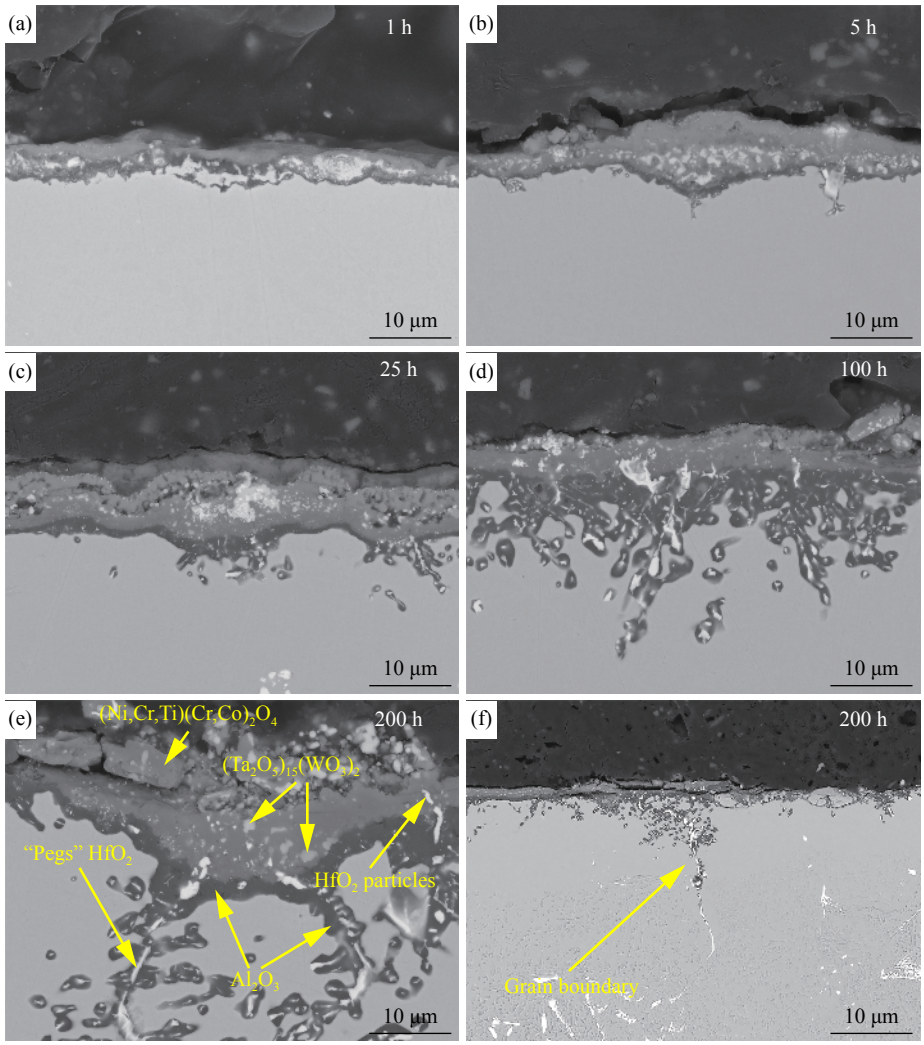

Fig. 7. SEM backscattered electron micrographs of cross section of the high Hf nickel-based superalloy after oxidation at 1100°C for (a) 1 h, (b) 5 h, (c) 25 h, (d) 100 h, and (e, f) 200 h.

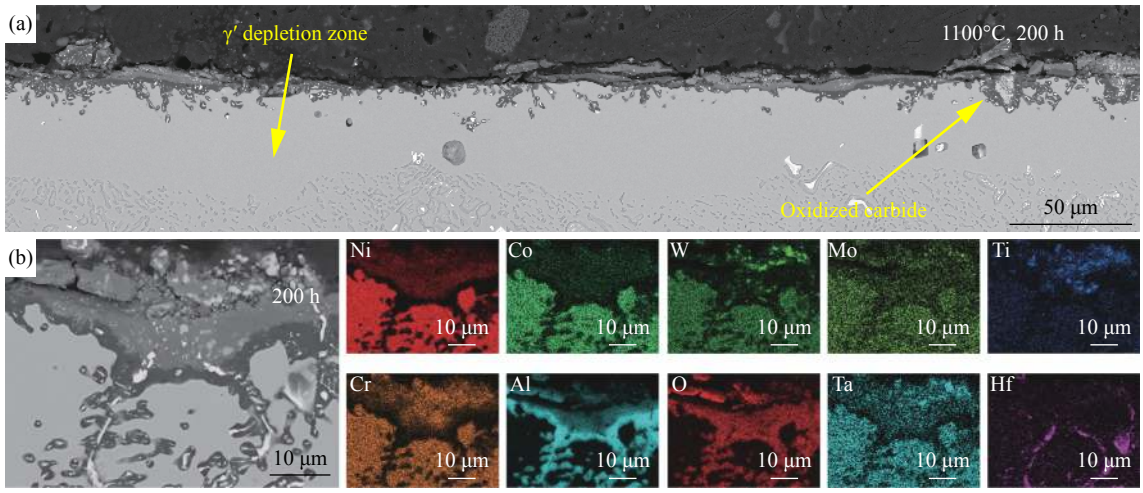

Fig. 8. Element distribution maps of cross section of the high Hf nickel-based superalloy after oxidation at 1100°C for 200 h: (a) microstructure morphology at low magnification; (b) noncarbide region.

ward for outward diffusion through high energy defects, such as vacancies, interfaces, and grain boundaries. This action led to the segregation of Hf cations at the high energy defect sites. Meanwhile, the O anions diffused inward rapidly along the grain boundaries in the oxide scale and combined with the Hf cations that segregated in the defects to form HfO_2. As for HfO_2, the conductivity of oxygen anions was higher than that of Al_2O_3 because of their defective crystal structure [39–40]. The O anions in HfO_2 easily reacted with the Al cations in the surrounding matrix to form an Al_2O_3 layer. The HfO_2 that formed in the defects acted as a core that continued to grow inward and subsequently exhibited a "peg-like" shape. Moreover, the carbides on the surface and subsurface were preferentially oxidized at 1000°C. The oxidation mechanism of the carbides on the surface at 1000°C was the same as that at 900°C. However, for the oxidized MC carbides on the subsurface, the principle of oxidation is attributable to the rapid inward diffusion of O anions to the carbide/matrix interface through the short-circuit diffusion of grain boundaries in the oxide scale, resulting in the reaction with Hf cations in carbides to form HfO_2. The HfO_2 that formed on the outer surface of the carbides acted as a fast transport medium for O anions, thereby continuously transforming the internal HfC into HfO_2.

Apart from the oxidation behavior at 900 and 1000°C, relatively small number of oxidized MC carbides and large amounts of "peg-like" HfO_2 appeared near the surface after oxidation at 1100°C. This result indicated the increasingly active diffusion of the Hf cations dissolved in the matrix. The effect is attributed to the increase in the diffusion driving force of the reactive elements caused by a rise in temperature. Hf cations can easily overcome energy barriers to achieve diffusion. The thickening of the γ′ depletion zone and the formation of Kirkendall pores are strong evidence of vigorous mutual diffusion [41]. More Hf cations dissolved at a deeper location of the matrix diffused outward promptly and segregated at high energy sites to form a "peg-like" HfO_2 cluster. The reduction of the oxidized surface of the MC carbides is probably due to the decomposition of some MC carbides into M_6C during the long-term isothermal exposure [42]. As O anions could not readily diffuse out of the dense Al_2O_3 layer wrapped by "peg-like" HfO_2, the carbides on the subsurface were hardly oxidized. A serious erosion of grain boundaries was also observed. As a result of the extremely high level of grain boundary energy, the grain boundary became a fast channel for oxygen anion diffusion. Vulnerable grain boundaries that are attacked during service may trigger crack initiation.

5. Conclusions

Based on the investigation of the effects of Hf on the oxidation behavior of the high Hf nickel-based superalloy at different temperatures, the following conclusions can be drawn. (1) In contrast to the oxidation at 900°C, HfO_2 particles formed within and beneath the oxide layer at 1000 and 1100°C. With increasing temperature, large amounts of "peg-like" HfO_2 formed. (2) HfO_2 formed as follows: Hf dissolved in the matrix was precipitated in situ, HfO_2 transformed from HfC, and "peg-like" HfO_2 was formed by diffusion. (3) The grain boundary can be used as a short-circuit channel of diffusion for oxygen anions and reactive element cations. This application increases the susceptibility to erosion at high temperatures.

Acknowledgements

This work was financially supported by the National Science and Technology Major Project (Nos. 2017-VI-0001-0070 and 2017-VI-0019-0091) and the National Natural Science Foundation of China (Nos. 51631008, 51771204, U1732131, 51671196, and 91860201).

References

[1] A.V. Logunov, S.A. Zavodov, and D.V. Danilov, The challenges in development of nickel-based heat-resistant superalloys for gas turbine disks and creation of a new superalloy with increased operational characteristics, *Mater. Today: Process.*, 11(2019), p. 459.

[2] F. Liu, Z.X. Wang, Z. Wang, J. Zhong, X.K. Wu, Z.J. Qin, Z.H. Li, L.M. Tan, L. Zhao, L.L. Zhu, L. Jiang, L. Huang, L.J. Zhang, and Y. Liu, High-throughput determination of interdiffusivity matrices in Ni−Al−Ti−Cr−Co−Mo−Ta−W multicomponent superalloys and their application in optimization of creep resistance, *Mater. Today Commun.*, 24(2020), art. No. 101018.

[3] P. Li, Q.Q. Li, T. Jin, Y.Z. Zhou, J.G. Li, X.F. Sun, and Z.F. Zhang, Effect of Re on low-cycle fatigue behaviors of Ni-based single-crystal superalloys at 900°C, *Mater. Sci. Eng. A*, 603(2014), p. 84.

[4] T. Zhu, C.Y. Wang, and Y. Gan, Effect of Re in γ phase, γ′ phase and γ/γ′ interface of Ni-based single-crystal superalloys, *Acta Mater.*, 58(2010), No. 6, p. 2045.

[5] Y.Q. Wang, M. Suneson, and G. Sayre, Synthesis of Hf-modified aluminide coatings on Ni-base superalloys, *Surf. Coat. Technol.*, 206(2011), No. 6, p. 1218.

[6] Z.X. Shi, J.R. Li, and S.Z. Liu, Effect of Hf on stress rupture properties of DD6 single crystal superalloy after long term aging, *J. Iron Steel Res. Int.*, 19(2012), No. 7, p. 66.

[7] Y.L. Tang, J.T. Liu, H.Y. Yu, Y.W. Zhang, J. Zhu, and H.W. Cheng, H.Y. Yu, Y.W. Zhang, and J. Zhu, Effect of hafnium on annealing twin formation in as-hot isostatically pressed nickel-based powder metallurgy superalloy, *J. Alloys Compd.*, 772(2019), p. 949.

[8] J. Romanowska, J. Morgiel, Ł. Kolek, P. Kwolek, and M. Zagula-Yavorska, Effect of Pd and Hf co-doping of aluminide coatings on pure nickel and CMSX-4 nickel superalloy, *Arch. Civ. Mech. Eng.*, 18(2018), No. 4, p. 1421.

[9] J.S. Hou, J.T. Guo, Y.X. Wu, L.Z. Zhou, and H.Q. Ye, Effect of hafnium on creep behavior of a corrosion resistant nickel base

superalloy, *Mater. Sci. Eng. A*, 527(2010), No. 6, p. 1548.
[10] T. Rangel-Ortiz, F.C. Alcala, V.M. López Hirata, J. Frias-Flores, J.E. Araujo-Osorio, H.J. Dorantes-Rosales, and M.L. Saucedo-Muñoz, Microstructure and tensile properties of a continuous-cast Al–Li–Hf alloy, *J. Mater. Process. Technol.*, 159(2005), No. 2, p. 164.
[11] H.W. Wang, J.X. Yang, J. Meng, Y.H. Yang, and Y.Z. Zhou, Wettability and interfacial reactions of a low Hf-containing nickel-based superalloy on Al_2O_3-based, SiO_2-based, $ZrSiO_4$, and $CoAl_2O_4$ substrates, *Ceram. Int.*, 46(2020), No. 14, p. 22057.
[12] X.Y. Chen, Y.Z. Zhou, T. Jin, and X.F. Sun, Effect of C and Hf contents on the interface reactions and wettability between a Ni_3Al-based superalloy and ceramic mould material, *J. Mater. Sci. Technol.*, 32(2016), No. 2, p. 177.
[13] F. Valenza, N. Sobczak, J. Sobczak, R. Nowak, M.L. Muolo, A. Passerone, S. Sitzia, and G. Cacciamani, Wetting and interfacial phenomena in Ni−Cr−Hf/sapphire systems, *J. Eur. Ceram. Soc.*, 40(2020), No. 2, p. 521.
[14] V.K. Tolpygo, K.S. Murphy, and D.R. Clarke, Effect of Hf, Y and C in the underlying superalloy on the rumpling of diffusion aluminide coatings, *Acta Mater.*, 56(2008), No. 3, p. 489.
[15] M. Zagula-Yavorska, J. Romanowska, M. Pytel, and J. Sieniawski, The microstructure and oxidation resistance of the aluminide coatings deposited by the CVD method on pure nickel and hafnium-doped nickel, *Arch. Civ. Mech. Eng.*, 15(2015), No. 4, p. 862.
[16] H.B. Guo, Y.J. Cui, H. Peng, and S.K. Gong, Improved cyclic oxidation resistance of electron beam physical vapor deposited nano-oxide dispersed β-NiAl coatings for Hf-containing superalloy, *Corros. Sci.*, 52(2010), No. 4, p. 1440.
[17] I.M. Allam, D.P. Whittle, and J. Stringer, The oxidation behavior of CoCrAI systems containing active element additions, *Oxid. Met.*, 12(1978), No. 1, p. 35.
[18] Y.Q. Wang and M. Suneson, Oxidation behavior of Hf-modified aluminide coatings on Haynes-188 at 1050°C, *Surf. Coat. Technol.*, 215(2013), p. 7.
[19] R. Baldan, R. Guimarães, C.A. Nunes, S.B. Gabriel, and G.C. Coelho, Oxidation behavior of the niobium-modified MAR-M247 superalloy at 1000°C in Air, *Oxid. Met.*, 83(2015), No. 1-2, p. 151.
[20] J. Wang, L.Z. Zhou, X.Z. Qin, L.Y. Sheng, J.S. Hou, and J.T. Guo, Primary MC decomposition and its effects on the rupture behaviors in hot-corrosion resistant Ni-based superalloy K444, *Mater. Sci. Eng. A*, 553(2012), p. 14.
[21] Y.S. Zhao, J. Zhang, Y.S. Luo, B. Zhang, G. Sha, L.F. Li, D.Z. Tang, and Q. Feng, Improvement of grain boundary tolerance by minor additions of Hf and B in a second generation single crystal superalloy, *Acta Mater.*, 176(2019), p. 109.
[22] C.T. Liu, J. Ma, and X.F. Sun, Oxidation behavior of a single-crystal Ni-base superalloy between 900 and 1000°C in air, *J. Alloy. Compd.*, 491(2010), No. 1-2, p. 522.
[23] L. Liu, Yi. Li, and F.H. Wang, Influence of micro-structure on oxidation Behavior of a ni-based superalloy at 1000°C, *Mater. Sci. Forum*, 595-598(2008), p. 87.
[24] A.M.S. Costa, E.S.N. Lopes, R.J. Contieri, R. Caram, R. Baldan, G.E. Fuchs, and C.A. Nunes, Microstructural and mechanical characterization of directionally solidified conventional and Nb-modified Mar-M247 superalloy, *J. Mater. Eng. Perform.*, 28(2019), No. 4, p. 2427.
[25] A. Sato, Y.L. Chiu, and R.C. Reed, Oxidation of nickel-based single-crystal superalloys for industrial gas turbine applications, *Acta Mater.*, 59(2011), No. 1, p. 225.
[26] L. Klein, A. Zendegani, M. Palumbo, S.G. Fries, and S. Virtanen, First approach for thermodynamic modelling of the high temperature oxidation behaviour of ternary γ′-strengthened Co−Al−W superalloys, *Corros. Sci.*, 89(2014), p. 1.
[27] H.Q. Pei, Z.X. Wen, Y.M. Zhang, and Z.F. Yue, Oxidation behavior and mechanism of a Ni-based single crystal superalloy with single α-Al_2O_3 film at 1000°C, *Appl. Surf. Sci.*, 411(2017), p. 124.
[28] H. Zhang, Y. Liu, X. Chen, H.W. Zhang, and Y.X. Li, Microstructural homogenization and high-temperature cyclic oxidation behavior of a Ni-based superalloy with high-Cr content, *J. Alloys Compd.*, 727(2017), p. 410.
[29] Y.F. Li, C. Li, L.M. Yu, Z.Q. Ma, H.J. Li, and Y.C. Liu, Characterization of γ′ precipitate and γ/γ′ interface in polycrystalline Ni_3Al-based superalloys, *Vacuum*, 176(2020), art. No. 109310.
[30] T.W. Huang, J. Lu, Y. Xu, D. Wang, J. Zhang, J.C. Zhang, J. Zhang, and L. Liu, Effects of rhenium and tantalum on microstructural stability of hot-corrosion resistant single crystal superalloys aged at 900°C, *Acta Metall. Sin.*, 55(2019), No. 11, p. 1427.
[31] H.A. Al-Abadleh, and V.H. Grassian, FT-IR study of water adsorption on aluminum oxide surfaces, *Langmuir*, 19(2003), No. 2, p. 341.
[32] K.P.R. Reddy, J.L. Smialek, and A.R. Cooper, ^{18}O tracer studies of Al_2O_3 scale formation on NiCrAl alloys, *Oxid. Met.*, 17(1982), No. 5/6, p. 429.
[33] B.A. Pint, J.R. Martin, and L.W. Hobbs, ^{18}O/SIMS characterization of the growth mmechanism of doped and undoped a-Al_2O_3, *Oxid. Met.*, 39(1993), No. 3/4, p. 167.
[34] W.J. Quadakkers, H. Holzbrecher, K.G. Briefs, and H. Beske, Differences in growth mechanisms of oxide scales formed on ODS and conventional wrought alloys, *Oxid. Met.*, 32(1989), No. 1/2, p. 67.
[35] C. Li, P. Song, A. Khan, J. Feng, K.L. Chen, J.J. Zang, X.P. Xiong, J.G. Lü, and J.S. Lu, Influence of water vapour on the HfO_2 distribution within the oxide layer on CoNiCrAlHf alloys, *J. Alloys Compd.*, 739(2018), p. 690.
[36] B.A. Pint and K.A. Unocic, Ionic segregation on grain boundaries in thermally grown alumina scales, *Mater. High Temp.*, 29(2012), No. 3, p. 257.
[37] X.Z. Cao, J. He, H. Chen, B.Y. Zhou, L. Liu, and H.B. Guo, The formation mechanisms of HfO_2 located in different positions of oxide scales on Ni−Al alloys, *Corros. Sci.*, 167(2020), art. No. 108481.
[38] B.A. Pint, A.J. Garratt-Reed, and L.W. Hobbs, Possible role of the oxygen potential gradient in enhancing diffusion of foreign ions on α-Al_2O_3 grain boundaries, *J. Am. Ceram. Soc.*, 81(1998), No. 2, p. 305.
[39] J. He, Z. Zhang, H. Peng, S.K. Gong, and H.B. Guo, The role of Dy and Hf doping on oxidation behavior of two-phase (γ' + β) Ni−Al alloys, *Corros. Sci.*, 98(2015), p. 699.
[40] H. Hindam and D.P. Whittle, Peg formation by short-circuit diffusion in Al_2O_3 scales containing oxide dispersions, *J. Electrochem. Soc.*, 129(1982), No. 5, p. 1147.
[41] A.E. Paz y Puente, and D.C. Dunand, Effect of Cr content on interdiffusion and Kirkendall pore formation during homogenization of pack-aluminized Ni and Ni−Cr wires, *Intermetallics*, 101(2018), p. 108.
[42] X.Z. Qin, J.T. Guo, C. Yuan, C.L. Chen, J.S. Hou, and H.Q. Ye, Decomposition of primary MC carbide and its effects on the fracture behaviors of a cast Ni-base superalloy, *Mater. Sci. Eng. A*, 485(2008), No. 1-2, p. 74.